Frequency Domain Synthesis of a Robust Flutter Suppression Control Law

D.K. Schmidt*
Purdue University, West Lafayette, Indiana
and
T.K. Chen†
Lear Siegler Inc., Dayton, Ohio

Computer-aided conventional synthesis techniques are employed to obtain a robust active-flutter-suppression control law. The relatively high dynamic order of such problems are dealt with effectively with a computer-aided approach, while computer graphics allows conventional graphical techniques to be utilized. Key design information is displayed for variations in flight conditions such that a simple control law is obtained that is robust over variations in the flight condition. Through visualization of the pole *and* zero migration with dynamic pressure, for example, control synthesis, evaluation of effects of unsteady aerodynamics and model reduction were performed almost by inspection. A candidate control law is analytically shown to compare very favorably to several others taken from the literature.

Introduction

TRADITIONALLY, passive methods such as increased structural stiffness, mass balancing, speed restriction, etc.,[1] have been used to eliminate flutter. However, such methods of flutter prevention add weight, leading to limited performance and reduced fuel economy. Therefore, there is a considerable interest in developing active control methods that can be used in place of, or in combination with, the traditional passive methods. As a result, a considerable number of analytical and experimental studies on active flutter suppression problems have been performed during the last decade utilizing a variety of synthesis techniques.[2-16] Recently, several investigations have concentrated on the application of multivariable state-space techniques.[5,13,14,16] But some shortcomings of this methodology, namely robustness and control-law complexity, prompt the utilization of a frequency-domain approach here.

There are several features of the aeroelastic control problem that must be dealt with: highly unstable plants, high-order dynamics, modeling uncertainty, and wide variability in operating conditions. The first arises from the desire to significantly increase the flutter speed, or to achieve high performance payoff. The high dynamic order is due to the usual inclusion of several elastic modes in the model, and the modeling of unsteady aerodynamic effects. Considerable uncertainty arises in the determination of the modal response and unsteady aerodynamics as well. The last two features lead to a requirement for a very robust control law.

Although the system model may be of relatively high order, the number of measurements and control inputs, or the number of transfer functions, may be very small. In such a case, the advantage of a multivariable synthesis technique is questionable. Therefore, this paper will focus on the utilization of more conventional synthesis approaches, but exercised interactively by means of computer graphics. The flutter-suppression control law synthesis will involve:

1) Graphical display of the pole and zero migration with flight condition (dynamic pressure) variations.

2) Use of the root-locus and Bode plots to synthesize a robust control law.

3) Evaluation of robustness with a Nyquist contour or the magnitude of the return difference $1+G(s)H(s)$.

4) Analytical comparison of the candidate control law to others obtained from the literature by a variety of techniques.

Computer software, much of it developed as part of this project, was exercised on a 16-bit minicomputer with graphical-display hardware (CRT) and hardcopy plot capability. All graphical information needed from items 1-3 above was then available for CRT display as well as plots such as those presented (though enhanced for clarity) in this paper.

The Elastic Wing Model

The differential equations of motion of a three-dimensional wing and control surfaces can be expressed in modal form as

$$M_i\ddot{q}_i(t)+2\zeta_i\omega_iM_i\dot{q}_i(t)+\omega_i^2M_iq_i(t)=-Q_i(t)$$

$$(i=1,2,\ldots n) \qquad (1)$$

where M_i is the generalized modal mass, $q_i(t)$ the generalized modal coordinate, and $Q_i(t)$ the generalized aerodynamic force, all associated with mode i. If these forces are considered to arise from elastic deformation, a scalar control deflection δ, and atmospheric turbulence w_g, one may obtain in matrix form

$$(Ms^2+Ds+K)\bar{q}_F(s)+qQ_F\bar{q}_F(s)$$

$$=-qQ_C\delta(s)-qQ_G[w_G(s)/V] \qquad (2)$$

where q is the dynamic pressure; $\bar{q}_F=[q_1,\ldots,q_n]^T$; M, D, and K are the generalized mass, damping, and stiffness matrices, respectively; and subscripts F, C, and G represent aerodynamic forces related to flexible modes, control surface deflection, and gust velocity, respectively. The s-plane approximations, $\hat{Q}_F$, $\hat{Q}_C$, $\hat{Q}_G$, to the unsteady aerodynamic force coefficient matrices Q_F, Q_C, Q_G, can be obtained by least-square curve-fitting numerical procedures.[15] Defining

Received Oct. 22, 1984; presented as Paper 85-0754 at the AIAA/ASME/ASCE/AHS 26th Structures, Structural Dynamics and Materials Conference, Orlando, FL, April 15-17, 1985; revision received Dec. 9, 1985.

*Professor, School of Aeronautics and Astronautics. Associate Fellow AIAA.

†Member of Technical Staff, Flight Systems Technology Department, Astronics Division. Member AIAA.

$\bar{q}_{A_j}$ = synthetic aerodynamic state vector, $(j=1,\ldots,L)$, and L the number of aerodynamic lag terms retained in the approximation, and

$$\bar{x}' = [\bar{q}_F^T, \dot{\bar{q}}_F^T, \bar{q}_{A_1}^T, \ldots, \bar{q}_{A_L}^T]^T \tag{3}$$

$$\bar{u}' = [\delta, \dot{\delta}, \ddot{\delta}]^T \tag{4}$$

$$w_G' = w_g/V \tag{5}$$

the equation of motion can be written in the state variable form as

$$\dot{\bar{x}}' = A'\bar{x}' + B\bar{u}' + Ew_G' \tag{6}$$

where the matrices $A' = f_1(M, D, K, q, \hat{Q}_F)$, $B = f_2(M, q, \hat{Q}_F, \hat{Q}_c)$, and $E = f_3(M, q, \hat{Q}_F, \hat{Q}_G)$, respectively.

The responses (e.g., accelerations) can be expressed as

$$\bar{y} = \Phi(x_s, y_s)\begin{bmatrix} C_1 & C_2 & C_3 \end{bmatrix}\begin{vmatrix} \bar{x}' \\ \bar{u}' \\ w_G' \end{vmatrix} \tag{7}$$

where $(x_s, y_s) = x, y$ coordinates of the sensor location, the matrix $\Phi(x_s, y_s)$ depends on the mode shapes, $\phi_i(x_s, y_s)$, or

$$\Phi(x_s, y_s) = [\phi_1(x_s, y_s) \mid \ldots\ldots \mid \phi_n(x_s, y_s)] \tag{8}$$

and C_1, C_2, C_3 are all functions of M, D, K, q, and $\hat{Q}$.

The actuator model is expressed as

$$\dot{\bar{x}}_a = A_a\bar{x}_a + B_a\bar{u}_c, \qquad \bar{u}' = C_a\bar{x}_a \tag{9}$$

where $\bar{x}_a$ = actuator state vector and $\bar{u}_c$ = actuator command input. The gust model is likewise expressed as

$$\dot{\bar{x}}_G = A_G\bar{x}_G + B_G w, \qquad \bar{w}_G' = C_G\bar{x}_G \tag{10}$$

where $\bar{x}_G$ = gust state vector and w = "white" stochastic process of intensity W. Then the overall open-loop aeroelastic system can be expressed as

$$\begin{vmatrix} \dot{\bar{x}}' \\ \dot{\bar{x}}_a \\ \dot{\bar{x}}_G \end{vmatrix} = \begin{vmatrix} A' & BC_a & EC_G \\ 0 & A_a & 0 \\ 0 & 0 & A_G \end{vmatrix}\begin{vmatrix} \bar{x}' \\ \bar{x}_a \\ \bar{x}_G \end{vmatrix} + \begin{vmatrix} 0 \\ B_a \\ 0 \end{vmatrix}\bar{u}_c + \begin{vmatrix} 0 \\ 0 \\ B_G \end{vmatrix} w \tag{11}$$

$$\bar{y} = \Phi(x_s, y_s)\begin{bmatrix} C_1 & C_2C_a & C_3C_G \end{bmatrix}\begin{vmatrix} \bar{x}' \\ \bar{x}_a \\ \bar{x}_G \end{vmatrix} \tag{12}$$

Such a state-variable representation is especially suitable for some numerical computations, such as evaluating the statistical performance [e.g., root-mean-square (rms) responses to turbulence] by a covariance analysis. However, the synthesis and system robustness evaluation utilize frequency-domain information depicted graphically, and the transfer functions are required. These transfer functions may be expressed as

$$\begin{aligned} Y(s) = \Phi(x_s, y_s)\{&[C_1(sI-A')^{-1}B + C_2] \\ &\times C_a(sI-A_a)^{-1}B_aU_c(s) + [C_1(sI-A')^{-1}E + C_3] \\ &\times C_G(sI-A_G)^{-1}B_GW(s)\} \end{aligned} \tag{13}$$

or

$$Y(s) = G_u(s)U_c(s) + G_g(s)W(s) \tag{14}$$

It is noted that only the transfer-function zeros are affected by sensor position (x_s, y_s) and actuator position (through changes in B). However, flight dynamic pressure and Mach number affect both zero and pole locations.

A control law of the form $U_c(s) = -H(s)Y(s)$ leads to the closed-loop transfer function

$$Y(s) = [I + G_u(s)H(s)]^{-1}G_g(s)W(s) \tag{15}$$

With a single control surface and a single measurement y, the return difference $I + G_uH$ is a scalar and of course determines closed-loop stability

The numerical model to be considered in this case study is for the DAST (Drones for Aerodynamic and Structural Testing), and is denoted DAST/ARW-1.[5] The wing geometry is shown in Fig. 1. It includes a hydraulically actuated trailing-edge control surface, with maximum surface displacement and rate capabilities of approximately 14 deg and 820 deg/s, respectively. The linear mathematical model consists of five structural elastic modes, ten synthetic unsteady aerodynamic states, $\bar{q}_A$, three actuator states, $\bar{x}_a$, and two gust states, $\bar{x}_G$, (using a Dryden gust model). The open-loop dynamic-pressure locus of roots of det $[sI-A'] = 0$ is shown in Fig. 2. Note this does not include the actuator and gust modes, and the data used are for Mach 0.9. The sensor and actuator locations are those as determined in Ref. 8.

Control Law Synthesis

Design Objectives

The basic design objective[5] is to provide over a 40% increase in flutter dynamic pressure at Mach 0.9. The uncon-

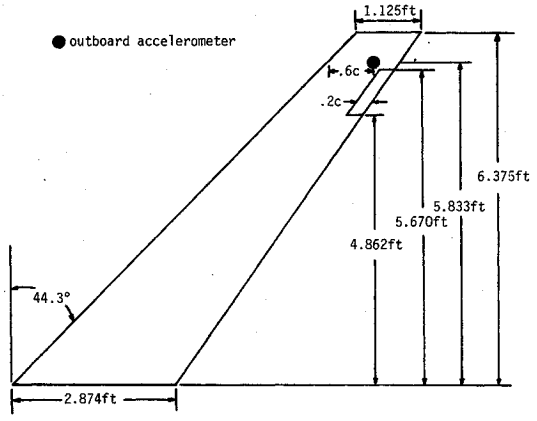

Fig. 1 Geometry of DAST wing model.

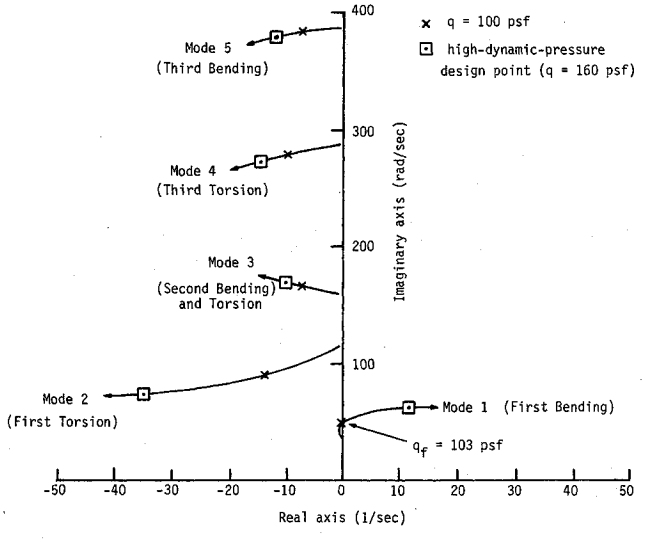

Fig. 2 Open-loop dynamic-pressure root locus at $M = 0.9$.

trolled flutter dynamic pressure is approximately 103 psf, as shown in Fig. 2. Furthermore (also as in Ref. 5) the rms control surface deflections δ_{rms} and rms rate $\dot{\delta}_{\text{rms}}$ are required to be lower than 6 deg and 350 deg/s, respectively, when evaluated with 1 ft/s rms (Dryden) turbulence, to avoid control saturation. The gain and phase margin are required to be at least ± 6 dB and ± 30 deg, respectively, and the measured acceleration is to be less than 1 g for good gust load alleviation purposes. At the same time, the overall system must be robust over all flight conditions, or the minimum of $|1+G_uH(j\omega)|$ is to be maximized over the range of dynamic pressure. Finally, for practical simplicity, the controller dynamic order is to be as low as possible.

Example at One Dynamic Pressure

Consider first the pole/zero locations depicted by the x's and circles, respectively, in Fig. 3. These data are for the high dynamic pressure (160 psf) condition, and represent the accelerometer-to-control-command transfer function $\ddot{z}/u_c$. The transfer-function zeros are determined by the method in Ref. 17, while the poles are the eigenvalues of the aeroelastic system and actuator matrices, A' and A_a, respectively.

Two zeros are at the origin, while two additional zeros (not shown) are at approximately $+300 \pm 2280j$. For generating the root-locus for this figure, these two zeros are significant, as shall be seen later. Note now that each pole associated with an unsteady aerodynamic root is almost cancelled by a neighboring zero. This is also the case for the pole/zero pairs for the third and fourth aeroelastic modes. Therefore, at least at this flight condition, these pole/zero pairs may be ignored for simplification in the control law synthesis. They cannot significantly affect the root locus but will be included in the complete evaluation model, as discussed later.

The gain root locus for this situation is as shown in Fig. 4a. Note the "actuator root" going unstable at higher gain, migrating toward the two far-away, right-half-plane zeros cited previously. Except for this mode, the *essence* of this problem is simply the adjustment of the characteristics of the key first and second elastic modes. Within the limitations already discussed, this is simply a fourth-order-system problem.

As shown in Fig. 4b, one can see that the flutter mode may be stabilized by a control law of the form

$$H(s) = K(s^2 + 2\zeta\omega_n s + \omega_n^2)/s^2 \qquad (16)$$

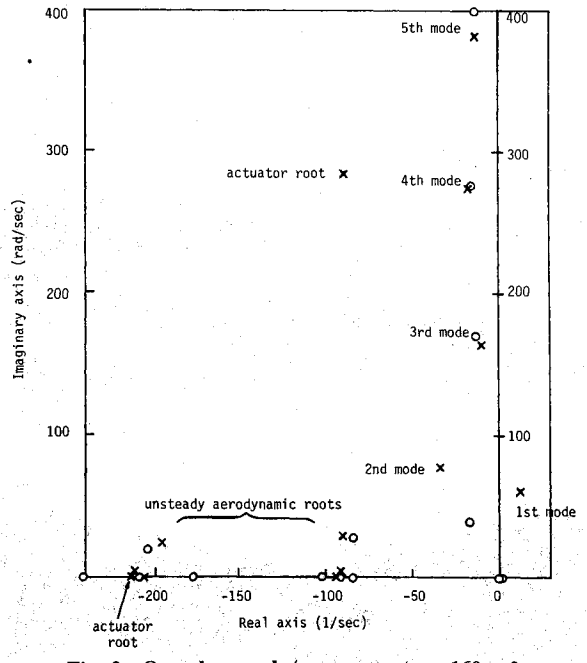

Fig. 3 Open-loop pole/zero map at $q = 160$ psf.

where the ζ and ω_n here determine the compensator zero locations. It is noted that the gain must be high enough to stabilize the unstable first mode, but is limited at the "high end" by the migration of the "actuator root." An additional pole at, say, -200 s^{-1}, could be added for attenuation of higher elastic modes, or the actuator could actually be slower.

Effect of Dynamic Pressure Variation

The real key to the problem is not a classical root locus for one flight condition. This was discussed at first primarily to "set the stage." The importance of the numerator locations cannot be overemphasized, however. Consider now the open-loop pole/zero locations shown in Fig. 5. This figure shows not only the migration of poles with dynamic pressure, but also the all-important zeros. The dynamic pressures range from 20 to 160 psf, by 20-psf increments. For each flight condition, there is near pole/zero cancellation for all unsteady aerodynamic poles, and for the third and fourth aeroelastic mode. Also, the fifth mode dipole has the same configuation, as considered previously. This mode, as well as the third mode, will be stabilized for these zero locations for all flight conditions shown with any reasonable gain. Consequently, the first and second modes are still the only truly important ones.

From this figure, one sees that by adroitly selecting compensator zeros in the region labeled CZ, these two modes may be stabilized, not only at the high dynamic pressure, as already

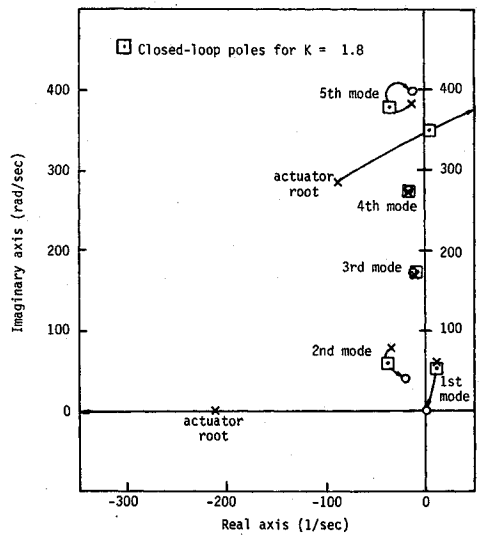

Fig. 4a A reduced-order root locus for acceleration output feedback.

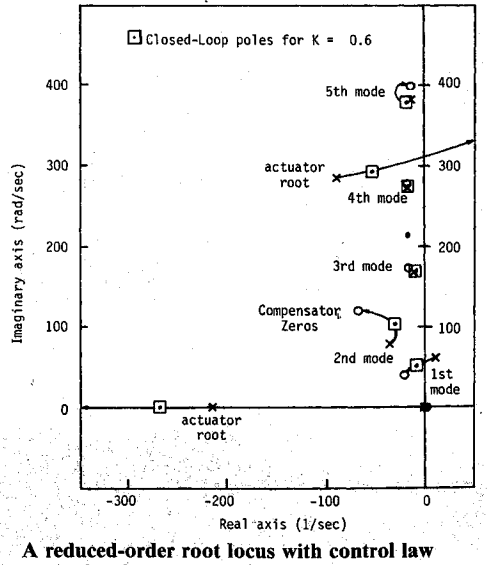

Fig. 4b A reduced-order root locus with control law $K(s^2 + 2\zeta\omega_n s + \omega_n^2)/s^2$.

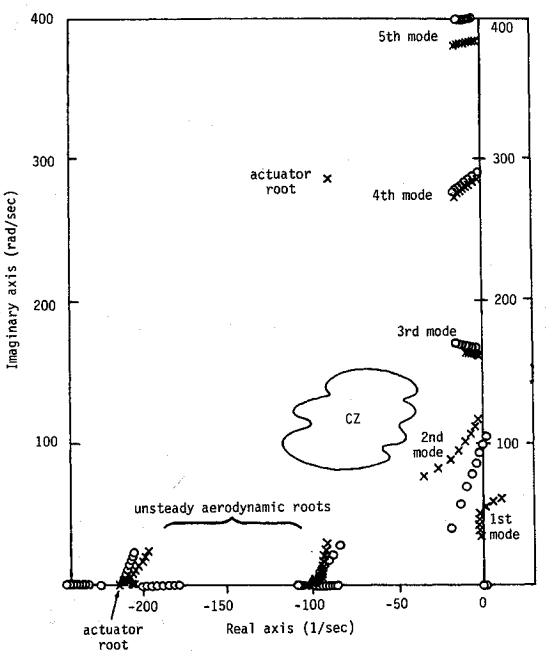

Fig. 5 Open-loop pole/zero map, $q = 20$-160 psf, 20 psf increments.

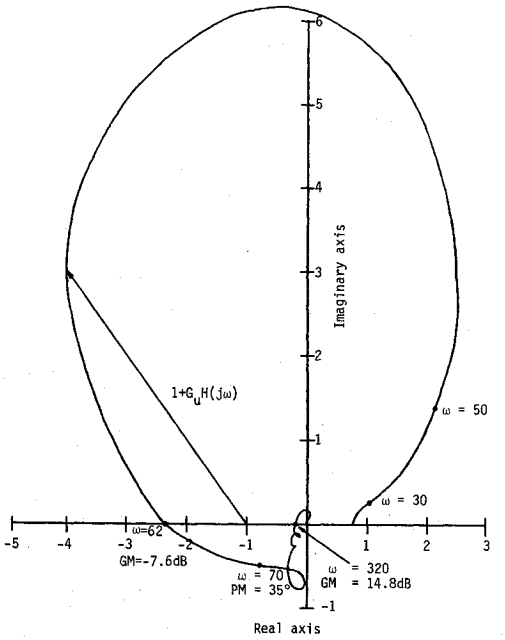

Fig. 6 Nyquist contour for $q = 120$ psf.

Table 1 Results of interactive design (evaluated with 25th-order plant)[a]

Dynamic pressure q, psf	$\ddot{z}_{rms}$, g	δ_{rms}, deg	$\dot{\delta}_{rms}$, deg/s	$\min_\omega \lvert 1 + G_u H(j\omega) \rvert$	GM, dB		PM, deg	
160	.76	4.63	202.3	.61	−6.38	8.76	−40.2	61.9
140	.69	3.53	166.8	.64	−7.79	10.0	−109.3	65.7
120	.62	2.84	141.8	.68	−13.62	11.41	−129.6	66.1
100	.49	2.20	109.1	.61	−	13.09	−126.8	35.6
80	.36	1.67	79.2	.50	−	14.55	−125.2	30.1
60	.24	1.28	56.3	.50	−	17.69	−125.8	30.4
40	.16	.95	38.7	.51	−	21.26	−129.3	31.4

[a] rms gust velocity = 1 ft/s.

Table 2 Comparison of results—25th-order plant model[a]

Controller design number	Order of controller	$\ddot{z}$, g	δ_{rms}, deg	$\dot{\delta}_{rms}$, deg/s	$\min_\omega \lvert 1 + G_u H(j\omega) \rvert$	GM, dB		PM, deg	
1	5	−[b]	3.85	207.7	.45	−5.48	5.21	−55.3	36.7
2	5	−	4.34	220.0	−	−6.00	13.60	−59.0	41.0
3	4	1.04	4.71	218.4	.69	−4.96	12.30	−45.3	53.0
4	2	.76	4.63	202.3	.61	−6.38	8.76	−40.2	61.9

[a] Dynamic pressure $q = 160$ psf; control surface activity constraint: $\delta_{rms} = 6$ deg, $\dot{\delta}_{rms} = 350$ deg/s; rms gust velocity = 1 ft/s. [b] Not available.

considered, but at lower dynamic pressures as well. This occurs due to the advantageous location of the zeros between the first and second mode pole locations. That is, for each flight condition shown, a *gain* root locus will show both the first and second mode could be stabilized. (And recall these zeros are affected by sensor locations.) Thus the information depicted graphically in this figure is enormous, and the utility of generating it with computer graphics should be apparent.

An adjustment to the compensator pole location to further enhance the robustness will now be addressed. Shown in Fig. 6 is the Nyquist contour for $G_u(s)H(s)$, with the compensator

$$H(s) = -[0.6[(s+67.5)^2 + 120^2]/s^2 \text{ deg}/g \qquad (17)$$

at the lower dynamic-pressure flight condition ($q = 120$ psf). Introducing less lag below 100 r/s or so rotates the contour counterclockwise, and the phase margins are improved. One resulting compensator is then

$$H(s) = -0.9[(s+67.5)^2 + 120^2]/(s+1)(s+26) \text{ deg}/g \qquad (18)$$

Control Law Evaluation

A covariance analysis, using the full 25th-order state model, was performed to evaluate the rms accelerations and control surface activities. Also, the minimum of the magnitude of the return difference $\lvert 1 + G_u H(j\omega) \rvert$, shown graphically in Fig. 6, was tabulated at each flight condition. The results are shown in Table 1. Note that the design objectives are met in each case.

Table 3 List of different reduced-order controller designs

Design no.	Reference no.	Controller form, deg/g
1	16	$\frac{-1.196(s^2+116.73s+7820)(s+22.91)}{(s+300)(s^2+73.63s+2829)(s^2+28.08s+362)}$
2	5	$\frac{-2214(s^2+30.79s+14692)(s^2+47.37s+72436)}{s(s^2+572.62s+88578)(s^2+568.59s+86972)}$
3	14	$\frac{-1939.4(s+24.74)(s^2+87.63s+13806)}{(s+3.864)(s+3270)(s^2+20.97s+1423)}$
4	This study	$\frac{-0.9(s^2135s+18956.25)}{(s+1)(s+26)}$

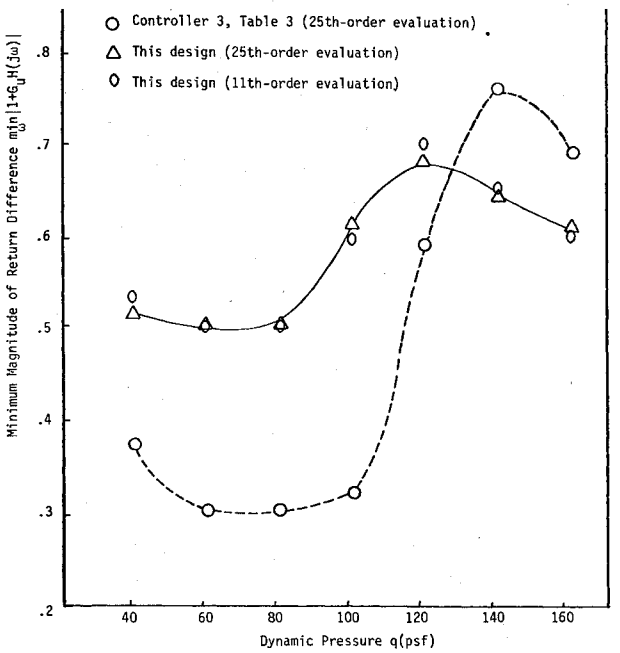

Fig. 7 Comparison of $\min_{\omega} |1+G_u H(j\omega)|$ at various flight conditions.

Shown in Table 2 are the comparable results for three other control laws proposed for this same wing model, obtained from the literature and evaluated in this analysis. The control laws being compared are listed in Table 3. Controllers 1-3 were obtained using three variations of optimal control theory. As can be seen from the results in Table 2, the controller obtained from this study (controller 4 in the table) compares very favorably with the other three at the design flight condition. The rms surface activities at this worst-case high dynamic pressure are quite similar, as well as the robustness evaluated at this design condition.

However, shown in Fig. 7 is the $\min |1+G_u H(j\omega)|$ evaluated over the range of dynamic-pressure conditions for controllers 3 and 4 in Table 3. As shown, the simpler second-order control law obtained from this graphical analysis is more robust over the dynamic-pressure range. Also shown is the result from evaluation of the candidate design using only an 11th-order evaluation model. This model is obtained by simply cancelling the unsteady aerodynamic poles and zeros as well as those associated with the third and fourth aeroelastic modes in the transfer function $G_u(s)$. As may be noted, the results are changed only slightly, thus tending to validate the model reduction by this method.

Summary

A simple, robust control law was synthesized with conventional techniques, aided with computer graphics. As shown, such a computer-aided classical control analysis program goes a long way toward overcoming the criticism that the graphical methods are too slow and cumbersome for higher-order systems.

The key significance of system zeroes was also demonstrated in this analysis. The role that the zero locations play in determining a system's limiting performance and stability were clearly exposed with classical Bode and root-locus techniques, and cannot be ignored. When compared to some control laws obtained from the literature, this control law compared favorably at the design condition, and the robustness was superior at off-design conditions. Such loss of robustness has been frequently cited as a key problem when time-domain multivariable technique, such as linear optimal control, are applied.

Acknowledgment

This work was supported in part by the NASA Langley Research Center under Grant NAG1-157. Mr. J.R. Newsom is the technical monitor.

References

[1]Shomber, H.A., "Application of Integrated Active Controls to Future Transports," AIAA Paper 79-1654, Aug. 1979.

[2]Triplett, W.E., "A Feasibility Study of Active Wing/Store Flutter Control," *Journal of Aircraft,* Vol. 9, June 1972, pp. 438-444.

[3]Sanford, M.C., Abel, I., and Gray, D.L., "Development and Demonstration of a Flutter Suppression System Using Active Controls," NASA TR R-450, 1975.

[4]Doggett, R.V. Jr., Abel, I., and Ruhlin, C.L., "Some Experiences Using Wind Tunnel Models in Active Control Studies," NASA TM X-3409, Aug. 1976, pp. 831-982.

[5]Newsom, J.R., Abel, I., and Dunn, H.J., "Application of Two Design Methods for Active Flutter Suppression and Wind-Tunnel Test Results," NASA TP-1653, May 1980.

[6]Abel, I. and Newsom, J.R., "Wind Tunnel Evaluation of NASA-Developed Control Laws for Flutter Suppression on a DC-10 Derivative Wing," AIAA Paper 81-0639, April 1981.

[7]Winther, B.A., Shirley, W.A., and Heimbaugh, R.M., "Wind-Tunnel Investigation of Active Controls Technology Applied to a DC-10 Derivative," *Journal of Guidance and Control,* Vol. 4, Sept.-Oct. 1981, pp. 536-542.

[8]Abel, I., Perry, P.B. III, and Murrow, H.N., "Two Synthesis Techniques Applied to Flutter Suppression on a Flight Research Wing," *Journal of Guidance and Control,* Vol. 1, Sept.-Oct. 1978, pp. 340-346.

[9]Noll, T.E. and Huttsell, L.J., "Wing Store Active Flutter Suppression Correlation of Analyses and Wind-Tunnel Data," *Journal of Aircraft,* Vol. 16, July 1979, pp. 491-497.

[10]Nissim, E., "Flutter Suppression Using Active Control Based on the Concept of Aerodynamic Energy," NASA TN D-6199, March 1971.

[11]Nissim, E., Capri, A., and Lottati, I., "Application of the Aerodynamic Energy Concept to Flutter Suppression and Gust Alleviation by Use of Active Controls," NASA TN D-8212, 1976.

[12]Nissim, E. and Lottati, I., "Active Controls for Flutter Suppression and Gust Alleviation in Supersonic Aircraft," *Journal of Guidance and Control,* Vol. 3, July-Aug. 1980, pp. 345-351.

[13]Gangsaas, D., Ly, U., and Norman, D.C., "Practical Gust loan Alleviation and Flutter Suppression Control Laws Based on a LQG Methodology," AIAA Paper 81-0021, Jan. 1981.

[14]Mukhopadhyay, V., Newsom, J.R., and Abel, I., "A Method for Obtaining Reduced-Order Control Laws for High-Order Systems Using Optimization Techniques," NASA TP 1876, Aug. 1981.

[15]Abel, I., "An Analytical Technique for Predicting the Characteristics of a Flexible Wing Equipped with an Active Flutter-Suppression System and Comparison with Wind-Tunnel Data," NASA TP-1367, 1979.

[16]Mahesh, J.K., Stone, C.R., Garrard, W.L., and Dunn, H.J., "Control Law Synthesis for Flutter Suppression Using Linear Quadratic Gaussian Theory," *Journal of Guidance and Control,* Vol. 4, July-Aug. 1981, pp. 415-422.

[17]Sandberg, I.W., and So., H.C., "A Two-Sets-of-Eigenvalues Approach to the Computer Analysis of Linear Systems," *IEEE Transactions on Circuit Theory,* Vol. CT-16, Nov. 1969.